



Substitution reactions of diiron dithiolate complexes with phosphine or isocyanide ligands

Xu-Feng Liu*

Department of Chemical Engineering, Ningbo University of Technology, Ningbo 315016, China



ARTICLE INFO

Article history:

Received 14 October 2013

Received in revised form

8 November 2013

Accepted 19 November 2013

Keywords:

Diiron dithiolate

Carbonyl substitution

Synthesis

Phosphine ligand

Crystal structure

ABSTRACT

A series of diiron dithiolate complexes bearing phosphine or isocyanide ligands, as the active site models of [FeFe]H₂ases, has been prepared by carbonyl substitution and structurally characterized. While complexes $[(\mu\text{-EDT})\text{Fe}_2(\text{CO})_5\text{L}_1]$ (EDT = SCH₂CH₂S, L₁ = PPh₃, **3**; Ph₂PCH₂PPh₂, **4**; ^tBuNC, **5**) were prepared by reactions of $(\mu\text{-EDT})\text{Fe}_2(\text{CO})_6$ (**1**) with PPh₃, Ph₂PCH₂PPh₂ (dpmm), or ^tBuNC in the presence of Me₃NO·2H₂O in MeCN in 52–82% yields, complex $(\mu\text{-EDT})\text{Fe}_2(\text{CO})_4(^t\text{BuNC})_2$ (**6**) was produced by reaction of **1** with 2 equivalents of ^tBuNC in CH₂Cl₂ in 42% yield. Treatment of **1** or $(\mu\text{-PDT})\text{Fe}_2(\text{CO})_6$ (PDT = SCH₂CH₂CH₂S) (**2**) with Me₃NO·2H₂O followed by addition of 4-PyN(PPh₂)₂ (Py = C₅H₄N) gave unexpected products $(\mu\text{-EDT})\text{Fe}_2(\text{CO})_5[\text{Ph}_2\text{PP}(\text{O})\text{Ph}_2]$ (**7**), $(\mu\text{-EDT})\text{Fe}_2(\text{CO})_5(\text{Ph}_2\text{PNHPy-4})$ (**8**), $(\mu\text{-PDT})\text{Fe}_2(\text{CO})_5[\text{Ph}_2\text{PP}(\text{O})\text{Ph}_2]$ (**9**), and $(\mu\text{-PDT})\text{Fe}_2(\text{CO})_5(\text{Ph}_2\text{PNHPy-4})$ (**10**) in 20–38% yields, respectively. In addition, the asymmetrically disubstituted complex $(\mu\text{-EDT})\text{Fe}_2(\text{CO})_4(\text{Ph}_2\text{PCH}_2\text{CH}_2\text{PPh}_2)$ (**11**) was obtained by reaction of **1** with Ph₂PCH₂CH₂PPh₂ (dppe) in refluxing xylene in 31% yield, whereas reaction of **2** with 1,1'-bis(diphenylphosphino)ferrocene (dppf) in refluxing xylene afforded the symmetrically disubstituted complex $(\mu\text{-PDT})\text{Fe}_2(\text{CO})_4[(\eta^5\text{-Ph}_2\text{PC}_5\text{H}_4)_2\text{Fe}]$ (**12**) in 28% yield. The complexes **3–9, 11**, and **12** were characterized by elemental analysis, IR, and NMR spectroscopy, as well as for **3–7, 9, 11**, and **12** by X-ray crystallography.

© 2013 Elsevier B.V. All rights reserved.

1. Introduction

Hydrogenases are metalloenzymes that can catalyze hydrogen metabolism in several microorganism [1–3]. On the basis of their metal content in the active site, hydrogenases can be classified as [FeFe]hydrogenases ([FeFe]H₂ases), [NiFe]hydrogenases ([NiFe]H₂ases), and [Fe]hydrogenases (Hmd) [4–8]. In recent years, [FeFe]H₂ases have received more attention than [NiFe]H₂ases and Hmd due to their highly efficiency in the production of hydrogen [9–12]. X-ray crystallographic studies revealed that the active site of [FeFe]H₂ases contains a butterfly [2Fe2S] cluster linked to a cubic [4Fe4S] cluster through the sulfur atom of a cysteinyl group [13,14]. The [4Fe4S] cluster is responsible for the electron transfer, whereas the [2Fe2S] cluster is responsible for the formation and activation of hydrogen. The [2Fe2S] cluster is bridged by a dithiolate ligand, CO, and CN[−] ligands. The bridging dithiolate was supposed to be propanedithiolate [15], azadithiolate [16], or oxadithiolate [17]. In addition, diiron ethanedithiolate complexes [18] were also prepared in order to mimic the active site of [FeFe]H₂ases because their

structures were very close to propanedithiolate model complexes. On the basis of structural information, a great variety of model complexes have been designed and structurally characterized, for example, $[\mu\text{-}(\text{SCH}_2)_2\text{O}]\text{Fe}_2(\text{CO})_4(\text{PMe}_3)_2$ [19], $[(\mu\text{-PDT})\text{Fe}_2(\text{CO})_5\text{L}_2]$ (L₂ = 1,4-dithiane, 1,4-dioxane) [20], $(\mu\text{-PDT})\text{Fe}_2(\text{CO})_4(\kappa^2\text{-PPh}_2\text{N}^{\text{Ph}}_2)$ [21], and $[(\mu\text{-SCH}_2)_2\text{Fe}_2(\text{CO})_5]_2(\text{NCH}_2\text{CH}_2\text{N})(\text{Ph}_2\text{PCH}_2\text{CH}_2\text{CH}_2\text{PPh}_2)$ [22].

In this paper, we report the synthesis, characterization, and crystal structures of diiron dithiolate complexes **3–12** related to the active site of [FeFe]H₂ases. We introduce PPh₃, dpmm, dppe, dppf, 4-PyNHPPh₂, Ph₂PP(O)Ph₂, and ^tBuNC to the parent complex **1** or **2** because the phosphine or isocyanide ligands can mimic the CN[−] ligand in the active site of [FeFe]H₂ases.

2. Results and discussion

2.1. Synthesis and characterization of complexes **3–6**

We found that treatment of the parent complex **1** with 1 equiv of the decarbonylating agent Me₃NO·2H₂O in MeCN followed by addition of PPh₃, dpmm, or ^tBuNC afforded $(\mu\text{-EDT})\text{Fe}_2(\text{CO})_5(\text{PPh}_3)$ (**3**), $(\mu\text{-EDT})\text{Fe}_2(\text{CO})_5(\text{Ph}_2\text{PCH}_2\text{PPh}_2)$ (**4**), and $(\mu\text{-EDT})\text{Fe}_2(\text{CO})_5(^t\text{BuNC})$ (**5**) in 82%, 78%, and 52% yields, respectively

* Tel./fax: +86 574 87089989.

E-mail address: nkxliu@126.com.

(Scheme 1). In addition, complex $(\mu\text{-EDT})\text{Fe}_2(\text{CO})_4(^t\text{BuNC})_2$ (**6**) could be prepared by reaction of **1** with 2 equiv of $^t\text{BuNC}$ in CH_2Cl_2 in 42% yield.

While complexes **3** and **4** were previously studied by Ellgen [23] and Hogarth [24], respectively, **5** and **6** were new complexes. Complexes **3**–**6** were characterized by elemental analysis and spectroscopy. The IR spectra of **3**–**6** showed three to four strong absorption bands in the range of 2047–1921 cm^{-1} for their terminal carbonyls and **5** and **6** showed one absorption band at about 2150 cm^{-1} for their terminal isocyanide ligands. The highest absorption bands of terminal carbonyls moved towards lower frequencies than that of complex **1** (2079 cm^{-1}) [25] due to the stronger electron-donating behavior of phosphine or isocyanide ligands than carbonyl group [26]. The ^1H NMR spectra of **3** and **4** displayed two doublets at about δ 1.9 and 1.3 ppm with a coupling constant $J = 8.0$ Hz for their SCH_2 groups, whereas **5** and **6** displayed one singlet at about δ 2.2 ppm for their SCH_2 groups. The $^{31}\text{P}\{\text{H}\}$ NMR spectra of **3** and **4** appeared as a singlet at δ 63.13 ppm and two doublets at δ 55.21, –25.69 ppm, respectively. In addition, the $^{13}\text{C}\{\text{H}\}$ NMR spectra of **3**–**6** exhibited three signals in the range of δ 215.45–206.73 ppm assigned to the terminal carbonyl groups and one signal at about 156 ppm for **5** and **6** assigned to the isocyanide ligands.

The molecular structures of **3**–**6** were characterized by X-ray crystal diffraction analysis. While the ORTEP views of **3**–**6** are depicted in Figs. 1–4, selected bond lengths and angles are given in Table 1. As shown in Figs. 1 and 2, complexes **3** and **4** both contain a $[\text{Fe}_2\text{S}]$ cluster bearing five carbonyls and one phosphine ligand. The phosphorus atoms of PPh_3 and dppm reside in an apical position of the octahedral geometry of the Fe_2 atom, in accordance with those phosphine-substituted diiron dithiolate complexes $\{[(\mu\text{-SCH}_2)_2\text{NCH}_2\text{CH}_2\text{OC(O)C}_6\text{H}_4\text{I-p}]\text{Fe}_2(\text{CO})_5\text{Ph}_2\text{PCH}_2\}$ [27] and $\{[(\mu\text{-SCH}_2)_2\text{NCH}_2\text{CO}_2\text{Me}]\text{Fe}_2(\text{CO})_5[\text{Ph}_2\text{PP(O)Ph}_2]\}$ [28], but different from complex $[(\mu\text{-SCH}_2)_2\text{CH}_2]\text{Fe}_2(\text{CO})_5(\text{Ph}_2\text{PCH}_2\text{PPH}_2)$ [29]. The $\text{Fe}_1\text{--Fe}_2$ bond lengths [2.5070(4) Å for **3** and 2.5092(9) Å for **4**] are close to that in **1** [2.505(2) Å] [30], which is indicating that the substitution of phosphine ligands does not affect the $\text{Fe}\text{--Fe}$ bond length.

As shown in Figs. 3 and 4, complexes **5** and **6** consist of one or two $^t\text{BuNC}$ ligands, respectively. In contrast to the crystal structure of $\text{Fe}_2(\mu\text{-SCH}_2)_2\text{S}(\text{CO})_5(^t\text{BuNC})$ [26] reported previously, the $^t\text{BuNC}$ ligand in **5** occupies an apical position of the Fe atom. However, two

Table 1
Selected bond lengths (Å) and angles ($^\circ$) for **3**–**6**.

	3	4	5	6
$\text{Fe}(1)\text{--S}(1)$	2.2568(5)	2.2540(12)	2.2662(17)	2.2491(7)
$\text{Fe}(1)\text{--S}(2)$	2.2520(6)	2.2545(11)	2.2662(17)	2.2482(7)
$\text{Fe}(1)\text{--Fe}(2)$	2.5070(4)	2.5092(9)	2.523(3)	2.5119(7)
$\text{S}(2)\text{--Fe}(1)\text{--S}(1)$	79.923(19)	79.93(4)	80.34(8)	80.38(2)
$\text{S}(2)\text{--Fe}(1)\text{--Fe}(2)$	56.212(14)	56.20(3)	56.18(5)	56.320(17)
$\text{S}(1)\text{--Fe}(1)\text{--Fe}(2)$	56.118(17)	56.08(3)	56.18(5)	55.951(19)
$\text{Fe}(2)\text{--S}(1)$				
$\text{Fe}(2)\text{--S}(2)$				
$\text{Fe}(2)\text{--P}(1)$				
$\text{S}(1)\text{--Fe}(2)\text{--S}(2)$				
$\text{S}(1)\text{--Fe}(2)\text{--Fe}(1)$				
$\text{S}(2)\text{--Fe}(2)\text{--Fe}(1)$				

	3	4	5	6
$\text{Fe}(2)\text{--S}(1)$	2.2532(6)	2.2546(10)	2.2664(17)	2.2588(7)
$\text{Fe}(2)\text{--S}(2)$	2.2369(6)	2.2508(10)	2.2664(17)	2.2450(7)
$\text{Fe}(2)\text{--P}(1)$	2.2245(11)	2.2245(11)	1.890(4)	1.880(2)
$\text{S}(1)\text{--Fe}(2)\text{--S}(2)$	80.00(16)	80.00(4)	80.34(8)	80.24(2)
$\text{S}(1)\text{--Fe}(2)\text{--Fe}(1)$	56.313(13)	56.23(3)	56.18(4)	56.070(19)
$\text{S}(2)\text{--Fe}(2)\text{--Fe}(1)$	56.164(17)	56.17(3)	56.18(4)	55.954(17)

$^t\text{BuNC}$ ligands in **6** both occupy an apical position of the Fe_1 and Fe_2 atoms, very similar to complex $\text{Fe}_2(\mu\text{-S}_2\text{C}_3\text{H}_6)(\text{CO})_4(^t\text{BuNC})_2$ [31]. The $\text{Fe}_1\text{--Fe}_2$ bond lengths [2.523(3) Å for **5** and 2.5119(7) Å for **6**] are consistent with those monoisocyanide or diisocyanide substituted diiron complexes $\text{Fe}_2(\mu\text{-S}_2\text{C}_3\text{H}_6)(\text{CO})_4(^t\text{BuNC})_2$ [2.5258(12) Å] [31], $\text{Fe}_2(\mu\text{-SCH}_2)_2\text{S}(\text{CO})_4(^t\text{BuNC})_2$ [2.5113(10) Å] [32], and $\text{Fe}_2(\mu\text{-SCH}_2)_2\text{S}(\text{CO})_5(^t\text{BuNC})$ [2.5313(5) Å] [26].

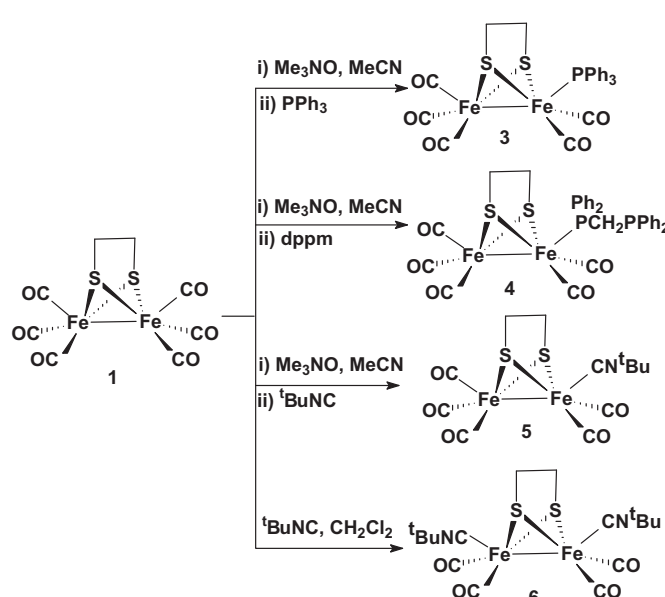
2.2. Synthesis and characterization of complexes **7**–**10**

As shown in Scheme 2, treatment of **1** or **2** with the decarbonylating agent $\text{Me}_3\text{NO}\cdot 2\text{H}_2\text{O}$ followed by addition of 4-PyN(PPh_2)₂ resulted in the formation of unexpected products **7**–**10** in 20%–38% yields, respectively. While **7**, **8**, and **9** were new complexes, **10** could also be prepared by reaction of **2** with 4-PyNHPPh₂ in the presence of $\text{Me}_3\text{NO}\cdot 2\text{H}_2\text{O}$ [33].

As reported recently, we have proposed a possible mechanism for the ligand rearrangement and oxidation reaction of diiron dithiolate complexes with 4-PyN(PPh_2)₂ (Scheme 3) [28]. While complexes **7** and **9** were obtained from ligand rearrangement and oxidation, complexes **8** and **10** were obtained from hydrolysis. However, the detailed mechanism still needed to be studied.

The new complexes **7**–**9** are air-stable solids, which have been characterized by elemental analysis, IR, and NMR spectroscopic techniques. The IR spectra of **7**–**9** showed three to four absorption bands in the region of 2044–1938 cm^{-1} for their terminal carbonyls. The ^1H NMR spectra of **8** displayed one doublet at δ 5.60 ppm with a coupling constant of $J_{\text{P-H}} = 17.0$ Hz for its NH group. The $^{31}\text{P}\{\text{H}\}$ NMR spectra of **7** and **9** demonstrated two doublets at about δ 55 and 34 ppm with coupling constants $J_{\text{P-P}} = 79.5$ and 72.6 Hz for one phosphorus coordinated to one Fe of the diiron subsite. In addition, the $^{13}\text{C}\{\text{H}\}$ NMR spectra of **8** and **9** exhibited a doublet and a singlet for their terminal carbonyls and three doublets and a singlet for their phenyl carbons.

The molecular structures of **7** and **9** were determined by single crystal X-ray diffraction analysis. While the ORTEP views are shown



Scheme 1. Synthesis of complexes **3**–**6**.

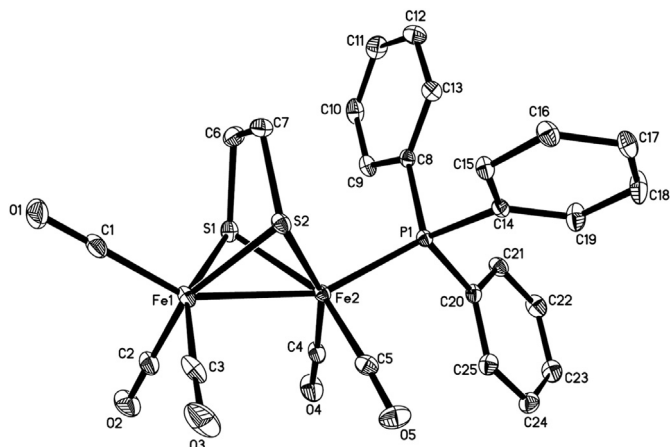


Fig. 1. ORTEP view of **3** with 30% probability level ellipsoids.

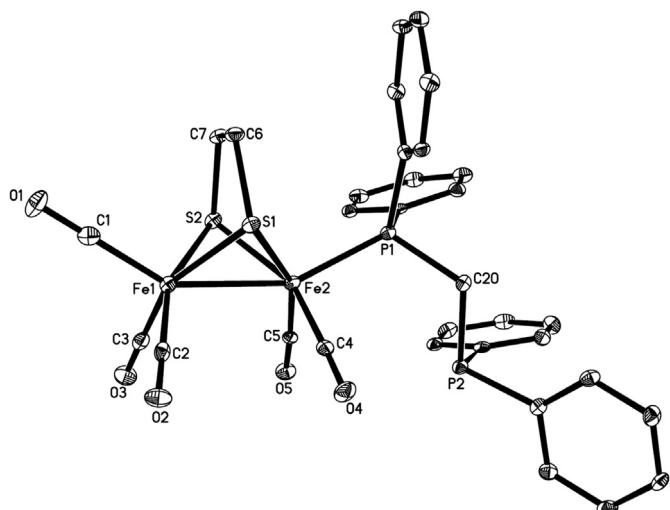


Fig. 2. ORTEP view of **4** with 30% probability level ellipsoids.

in Figs. 5 and 6, selected bond lengths and angles are presented in Table 2. As shown in Figs. 5 and 6, complexes **7** and **9** both contain a butterfly [2Fe2S] cluster with five carbonyls and one Ph₂PP(O)Ph₂ ligand. The diiron propanedithiolate moiety has two fused six-membered rings, in which one six-membered ring

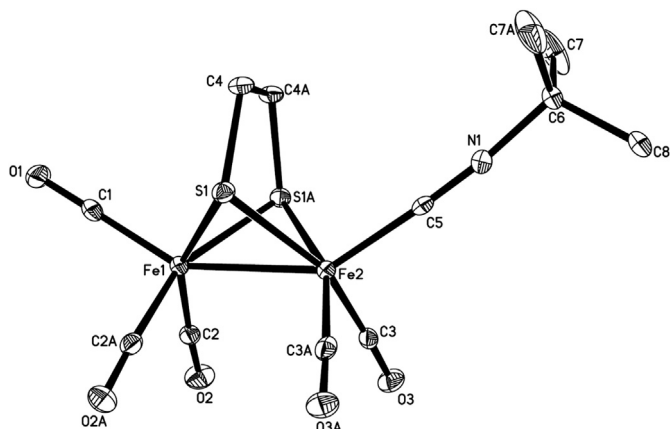


Fig. 3. ORTEP view of **5** with 30% probability level ellipsoids.

C7C6S1Fe2S2C8 has a boat conformation and the other six-membered ring C7C6S1Fe1S2C8 has a chair conformation, whereas the diiron ethanedithiolate moiety has two similar five-membered rings. The phosphorus atom of Ph₂PP(O)Ph₂ occupies an apical position of the square-pyramidal coordination sphere of the Fe₂ atom, in accordance with those monophosphine substituted diiron dithiolate complexes [34]. The Fe₁–Fe₂ bond length of **9** [2.5225(6) Å] is longer than its parent complex **2** [2.5103(11) Å] [15a] and other all-carbonyl diiron dithiolate complexes such as [(μ-SCH₂)₂NCH₂C₆H₄Br-*p*]Fe₂(CO)₆ [2.5083(7) Å] [35], but somewhat shorter than those in the structures of natural enzymes *Clostridium pasteurianum* and *Desulfovibrio desulfuricans* (2.55–2.62 Å) [13,14]. However, the Fe₁–Fe₂ bond length of **7** [2.5014(8) Å] is similar to its parent complex **1** [2.505(2) Å] [30]. All carbon atoms of carbonyls are about 1.77–1.80 Å apart from the iron atoms with some differences in their basal and apical positions due to the influence of phosphine ligand.

2.3. Synthesis and characterization of complexes **11** and **12**

As shown in Scheme 4, treatment of **1** with dppe in xylene at reflux resulted in formation of the corresponding asymmetrically disubstituted complex **11** in 31% yield, whereas reaction of **2** with dppf in xylene at reflux gave the symmetrically disubstituted complex **12** in 28% yield.

The new complexes **11** and **12** are air-stable solids, which have been characterized by elemental analysis and spectroscopy. The IR spectra of **11** and **12** showed four strong absorption bands in the region of 2017–1890 cm⁻¹ assigned to the terminal carbonyls, which are shifted towards lower frequencies relative to their parent complexes **1** (2079, 2039, 2009, 1996 cm⁻¹) [25] and **2** (2072, 2033, 1993 cm⁻¹) [15a]. The ³¹P{¹H} NMR spectra of **11** displayed only a singlet at 91.58 ppm whereas complex (μ-PDT)Fe₂(CO)₄(κ²-dppe) displayed two singlets at δ 89.6 and 75.0 ppm at room temperature in CD₂Cl₂ [36]. The results can be explained by the following reasons: (1) there are only two isomers (ba-ap and ba-ba) of **11** in solution (Scheme 5) because the EDT-type diiron complexes cannot rotate like PDT-type diiron complexes in solution [36] which is showing the only difference between EDT and PDT; (2) two phosphorus atoms of dppe are equivalent by interconversion in two isomers at room temperature in CDCl₃ [22]. The ¹H NMR spectra of **12** exhibited four singlets at δ 4.93, 4.46, 4.45, and 4.01 ppm for its two Cp ring hydrogens. The ³¹P{¹H} NMR spectra of **12** demonstrated a singlet at δ 50.85 ppm for the two phosphorus atoms of dppf, each one coordinated to one Fe of the diiron subsite.

In order to confirm the molecular structure of complexes **11** and **12**, single crystal X-ray diffraction analysis was undertaken. While the ORTEP views are shown in Figs. 7 and 8, selected bond lengths

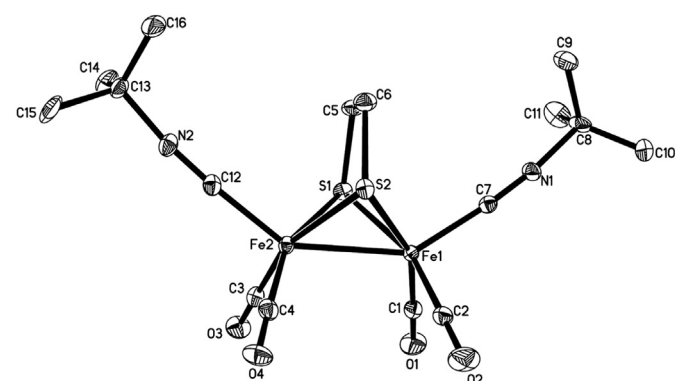
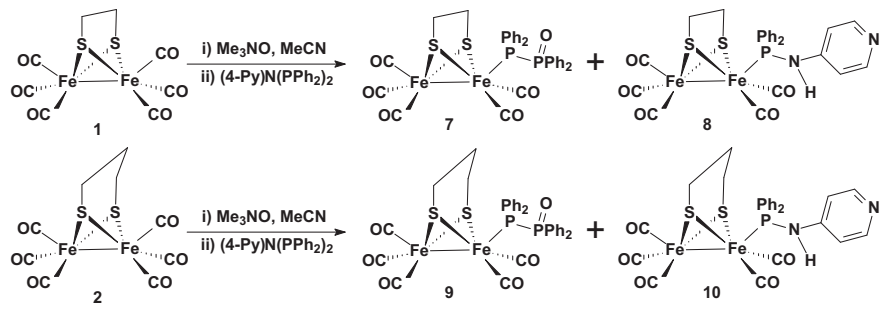
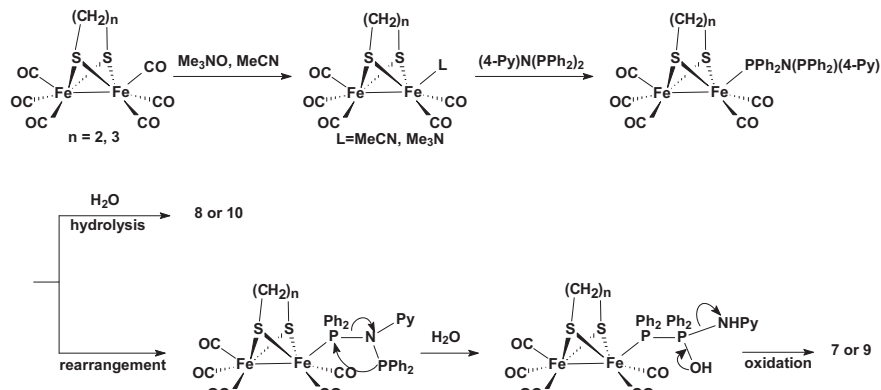


Fig. 4. ORTEP view of **6** with 30% probability level ellipsoids.



Scheme 2. Synthesis of complexes 7–10.



Scheme 3. Proposed mechanism for formation of complexes 7–10.

and angles are presented in Table 3. As depicted in Fig. 7, complex **11** consists of a butterfly [2Fe₂S] cluster with four carbonyls, a chelating dppe ligand and an ethylene group. Two phosphorus atoms reside in a basal–apical position of the square–pyramidal coordination sphere of Fe₂ atom, consistent with the crystal structures of (μ -PDT)Fe₂(CO)₄(κ^2 -dppe) [36] and Fe₂(CO)₄(κ^2 -dppe){ μ -SCH₂N(R)CH₂S} (R = ¹Pr, CH₂CH₂OMe, CH₂C₆H₅) [37], but different from (μ -PDT)Fe₂(CO)₄(κ^2 -dmpe) (dmpe = Me₂PC H₂CH₂PM₂) [38]. The Fe₁–Fe₂ bond length [2.5296(9) Å] is longer than that in **1** [2.505(2) Å] [30] and all-carbonyl diiron complexes, for example, [$(\mu$ -SCH₂)₂NCH₂CH₂OC(O)C₆H₄l-p]Fe₂(CO)₆ [2.5148 (1) Å] [27], but shorter than the Fe–Fe distance in (μ -PNT)Fe₂(CO)₆

(PNT = phenanthrene-4,5-dithiolate) [2.5365(7) Å] [39]. The average Fe–S bond length is 2.2612 Å and the Fe–S–Fe bond angles are 68.14 and 67.91°. The Fe₂–C₄ bond length [1.755(5) Å] is shorter than Fe₁–C bond lengths (1.783–1.792 Å) due to the substitution of a chelating bidentate phosphine ligand dppe.

As shown in Fig. 8, complex **12** contains a butterfly [2Fe₂S] cluster with four carbonyls and an intramolecular bridging dppf ligand. Two phosphorus atoms of dppf reside in a basal–basal position of the square–pyramidal coordination sphere of Fe₁ and Fe₂ atoms, similar to those previously reported diphosphine substituted diiron dithiolate complexes [29]. It is worth to point out that the bond length of Fe₁–Fe₂ [2.6165(10) Å] is much longer than that of **2** [2.5103(11) Å] [15a], but very close to those in the oxidized form of the natural enzymes (2.60 and 2.62 Å) [13,14].

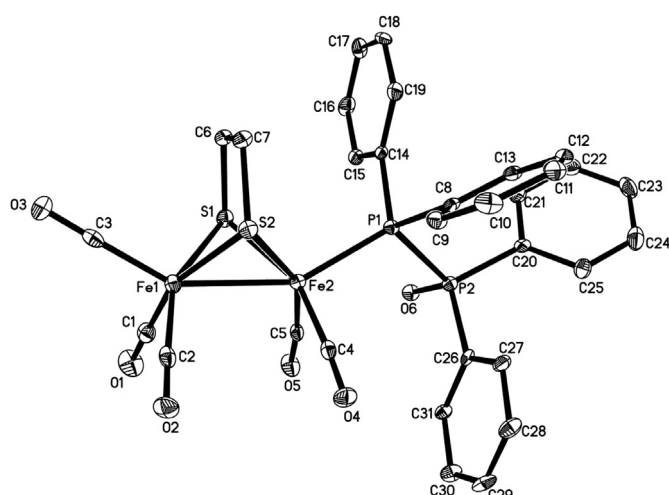


Fig. 5. ORTEP view of 7 with 30% probability level ellipsoids.

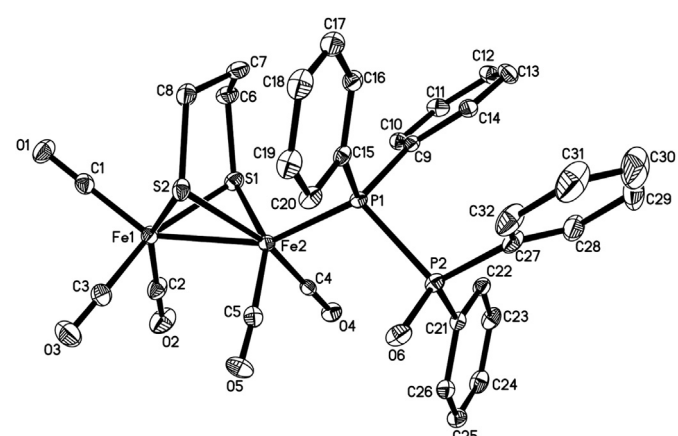


Fig. 6. ORTEP view of 9 with 30% probability level ellipsoids.

Table 2
Selected bond lengths (Å) and angles (°) for **7** and **9**.

	7	9	
Fe(1)–S(2)	2.2575(10)	Fe(2)–S(2)	2.2546(10)
Fe(1)–S(1)	2.2476(10)	Fe(2)–S(1)	2.2523(10)
Fe(1)–Fe(2)	2.5014(8)	P(1)–P(2)	2.2414(12)
Fe(2)–P(1)	2.2268(11)	P(2)–O(6)	1.4934(18)
S(2)–Fe(1)–S(1)	80.05(4)	P(1)–Fe(2)–S(1)	102.29(3)
S(2)–Fe(1)–Fe(2)	56.28(3)	S(2)–Fe(2)–S(1)	80.01(4)
S(1)–Fe(1)–Fe(2)	56.32(3)	P(1)–Fe(2)–Fe(1)	150.79(3)
S(1)–Fe(2)–Fe(1)	56.14(2)	S(2)–Fe(2)–Fe(1)	56.39(3)

3. Experimental

3.1. General comments

All reactions were performed using standard Schlenk and vacuum-line techniques under N₂ atmosphere. Acetonitrile and dichloromethane were distilled over CaH₂ under N₂. Xylene was distilled over sodium under N₂. Me₃NO·2H₂O, PPh₃, dppm, dppe, ^tBuNC, and other materials were available commercially and used as received. **1** [25], **2** [15a], 4-PyN(PPh₃)₂ [40], and dppf [41] were prepared according to literature procedures. IR spectra were recorded on a Nicolet MAGNA 560 FTIR spectrometer. NMR spectra were obtained on a Bruker Avance 400 or 500 MHz spectrometer. Elemental analyses were performed by a Perkin–Elmer 240C analyzer.

3.2. Preparation of (μ -EDT)Fe₂(CO)₅(PPh₃) (**3**)

To a solution of **1** (0.186 g, 0.5 mmol) in MeCN (15 mL) was added a solution of Me₃NO·2H₂O (0.056 g, 0.5 mmol) in MeCN (10 mL). The mixture was stirred at room temperature for 15 min and then PPh₃ (0.131 g, 0.5 mmol) was added. The new mixture was stirred for 1 h to give a red solution. The solvent was reduced *in vacuo* and the residue was subjected to TLC separation using CH₂Cl₂/petroleum ether (v/v = 1:3) as eluent. Collecting the main red band afforded 0.248 g (82%) of **3** as a red solid. Anal. Calc. for

C₂₅H₁₉Fe₂O₅PS₂: C, 49.53; H, 3.16. Found: C, 49.68; H, 3.24%. IR (KBr disk): $\nu_{C\equiv O}$ 2038vs, 1988vs, 1971vs, 1928vs cm⁻¹. ¹H NMR (500 MHz, CDCl₃): 7.59–7.41 (m, 15H, Ar–H), 1.86 (d, J = 8.0 Hz, 2H, SCH₂), 1.13 (d, J = 8.0 Hz, 2H, SCH₂) ppm. ³¹P{¹H} NMR (200 MHz, CDCl₃, 85% H₃PO₄): δ 63.13 (s) ppm. ¹³C{¹H} NMR (125 MHz, CDCl₃): δ 214.89, 214.82, 210.09 (C≡O), 136.05, 135.74, 133.17, 133.08, 130.20, 128.64, 128.56 (Ar–C), 34.85 (CH₂) ppm.

3.3. Preparation of (μ -EDT)Fe₂(CO)₅(Ph₂PCH₂PPh₂) (**4**)

The procedure was similar to that of **3** except Ph₂PCH₂PPh₂ (0.192 g, 0.5 mmol) was used instead of PPh₃. 0.284 g (78%) of **4** was obtained as a red solid. Anal. Calc. for C₃₂H₂₆Fe₂O₅PS₂: C, 52.77; H, 3.60. Found: C, 52.98; H, 3.30%. IR (KBr disk): $\nu_{C\equiv O}$ 2044vs, 1982vs, 1926vs cm⁻¹. ¹H NMR (500 MHz, CDCl₃): 7.54–7.19 (m, 20H, Ar–H), 3.25 (d, J = 6.5 Hz, 2H, PCH₂), 1.90 (d, J = 8.0 Hz, 2H, SCH₂), 1.38 (d, J = 8.0 Hz, 2H, SCH₂) ppm. ³¹P{¹H} NMR (200 MHz, CDCl₃, 85% H₃PO₄): 55.21 (d, J_{p-p} = 83.0 Hz), -25.69 (d, J_{p-p} = 84.2 Hz) ppm. ¹³C{¹H} NMR (125 MHz, CDCl₃): 215.45, 215.37, 210.11 (C≡O), 138.19, 138.13, 138.07, 138.01, 136.38, 136.35, 132.91, 132.74, 132.40, 132.32, 130.17, 128.69, 128.46, 128.41, 128.33, 128.25 (Ar–C), 34.97, 31.61 (CH₂) ppm.

3.4. Preparation of (μ -EDT)Fe₂(CO)₅(^tBuNC) (**5**)

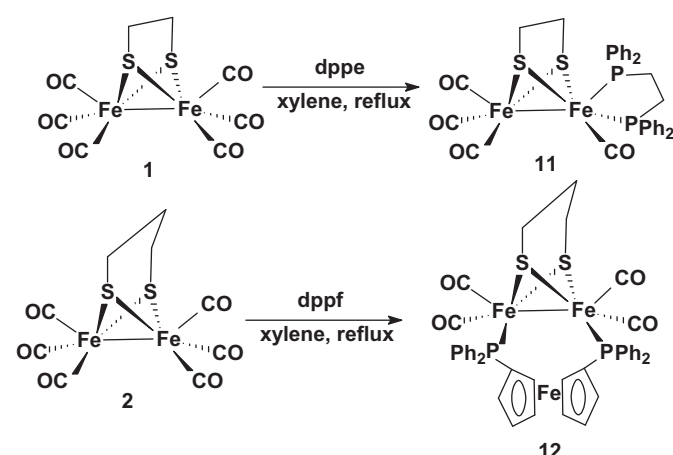
The procedure was similar to that of **3** except ^tBuNC (0.056 mL, 0.5 mmol) was used instead of PPh₃. 0.111 g (52%) of **5** was obtained as a red solid. Anal. Calc. for C₁₂H₁₃Fe₂NO₅S₂: C, 33.75; H, 3.07; N, 3.28. Found: C, 33.54; H, 3.29; N, 3.12%. IR (KBr disk): $\nu_{C\equiv N}$ 2153s; $\nu_{C\equiv O}$ 2047vs, 1986vs, 1950s cm⁻¹. ¹H NMR (500 MHz, CDCl₃): 2.25 (s, 4H, 2SCH₂), 1.47 (s, 9H, 3CH₃) ppm. ¹³C{¹H} NMR (125 MHz, CDCl₃): 213.75, 213.61, 210.44 (C≡O), 154.93 (NC), 57.98 (C(CH₃)₃), 35.95 (CH₂), 30.67 (CH₃) ppm.

3.5. Preparation of (μ -EDT)Fe₂(CO)₄(^tBuNC)₂ (**6**)

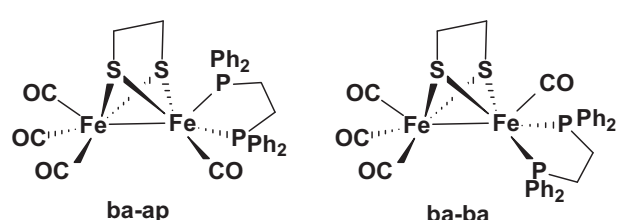
To a solution of **1** (0.186 g, 0.5 mmol) in CH₂Cl₂ (20 mL) was added ^tBuNC (0.112 mL, 1 mmol). The new mixture was stirred for 24 h at room temperature. The solvent was reduced *in vacuo* and the residue was subjected to TLC separation using CH₂Cl₂/petroleum ether (v/v = 1:2) as eluent. Collecting the main red band afforded 0.102 g (42%) of **6** as a red solid. Anal. Calc. for C₁₆H₂₂Fe₂N₂O₄S₂: C, 39.86; H, 4.60; N, 5.81. Found: C, 39.75; H, 4.42; N, 6.01%. IR (KBr disk): $\nu_{C\equiv N}$ 2141s; $\nu_{C\equiv O}$ 1998vs, 1948vs, 1921vs cm⁻¹. ¹H NMR (500 MHz, CDCl₃): 2.14 (s, 4H, 2SCH₂), 1.46 (s, 18H, 6CH₃) ppm. ¹³C{¹H} NMR (125 MHz, CDCl₃): 214.98, 212.65, 206.73 (C≡O), 158.87 (NC), 57.37 (C(CH₃)₃), 35.30 (CH₂), 30.80 (CH₃) ppm.

3.6. Preparation of (μ -EDT)Fe₂(CO)₅[Ph₂PP(O)Ph₂] (**7**) and (μ -EDT)Fe₂(CO)₅(Ph₂PNHPy-4) (**8**)

To a solution of **1** (0.372 g, 1 mmol) in MeCN (30 mL) was added a solution of Me₃NO·2H₂O (0.111 g, 1 mmol) in MeCN (15 mL). The



Scheme 4. Synthesis of complexes **11** and **12**.



Scheme 5. Two isomers (ba-ap and ba-ba) of **11** in solution.

Table 3
Selected bond lengths (Å) and angles (°) for **11** and **12**.

	Fe(1)–S(2)	Fe(2)–S(2)	2.2582(12)
Fe(1)–S(1)	2.2641(12)	Fe(2)–S(1)	2.2516(12)
Fe(1)–Fe(2)	2.5296(9)	Fe(2)–P(2)	2.1829(12)
Fe(2)–P(1)	2.2253(12)	C(23)–C(24)	1.535(5)
S(1)–Fe(1)–S(2)	79.39(4)	P(2)–Fe(2)–P(1)	89.10(5)
S(1)–Fe(2)–S(2)	79.92(4)	P(2)–Fe(2)–Fe(1)	154.66(4)
S(1)–Fe(1)–Fe(2)	55.70(3)	Fe(2)–S(1)–Fe(1)	68.14(4)
S(2)–Fe(1)–Fe(2)	55.81(3)	Fe(2)–S(2)–Fe(1)	67.91(4)
12			
Fe(1)–S(2)	2.2445(10)	Fe(2)–S(2)	2.2510(10)
Fe(1)–S(1)	2.2569(9)	Fe(2)–S(1)	2.2580(9)
Fe(1)–Fe(2)	2.6165(10)	Fe(2)–P(2)	2.2672(10)
Fe(1)–P(1)	2.2266(10)	Fe(1)–C(1)	1.766(3)
S(2)–Fe(1)–S(1)	84.22(4)	S(2)–Fe(2)–Fe(1)	54.29(2)
S(2)–Fe(1)–Fe(2)	54.52(3)	S(2)–Fe(2)–S(1)	84.04(3)
S(1)–Fe(1)–Fe(2)	54.60(2)	P(2)–Fe(2)–Fe(1)	118.65(3)
P(1)–Fe(1)–Fe(2)	120.11(4)	Fe(1)–S(1)–Fe(2)	70.84(3)
S(1)–Fe(2)–Fe(1)	54.56(3)	Fe(1)–S(2)–Fe(2)	71.19(3)

mixture was stirred at room temperature for 15 min and then was added 4-PyN(PPh₂)₂ (0.462 g, 1 mmol). The new mixture was stirred overnight to give a red solution. The solvent was reduced *in vacuo* and the residue was subjected to TLC separation using ethyl acetate/petroleum ether (*v/v* = 1:1) as eluent. Collecting the first red band afforded 0.153 g (21%) of **7** as a red solid. Collecting the second red band afforded 0.199 g (32%) of **8** as a red solid. **7**: Anal. Calc. for C₃₁H₂₄Fe₂O₆P₂S₂: C, 50.99; H, 3.31. Found: C, 51.28; H, 3.20%. IR (KBr disk): ν_{C≡O} 2044vs, 1986vs, 1975vs, 1938vs cm⁻¹. ¹H NMR (500 MHz, CDCl₃): 7.40–7.39 (m, 20H, Ar–H), 1.86–1.40 (m, 4H, 2CH₂) ppm. ³¹P{¹H} NMR (200 MHz, CDCl₃, 85% H₃PO₄): 54.33 (d, J_{P–P} = 72.6 Hz), 33.94 (d, J_{P–P} = 72.6 Hz) ppm. ¹³C{¹H} NMR (125 MHz, CDCl₃): 213.45, 209.72 (C≡O), 134.51, 132.61, 131.19, 128.47 (Ar–C), 35.13 (CH₂) ppm. **8**: Anal. Calc. for C₂₄H₁₉Fe₂N₂O₅PS₂: C, 46.33; H, 3.08; N, 4.50. Found: C, 46.58; H, 3.24; N, 4.58%.

IR (KBr disk): ν_{C≡O} 2044vs, 1981vs, 1938vs cm⁻¹. ¹H NMR (500 MHz, CDCl₃): 8.17 (br, 2H, Ar–H), 7.70, 7.46 (2s, 10H, Ar–H), 6.44 (s, 2H, Ar–H), 5.60 (d, J_{P–H} = 17.0 Hz, 1H, NH), 1.96 (d, J = 8.0 Hz, 2H, SCH₂), 1.42–1.41 (m, 2H, SCH₂) ppm. ³¹P{¹H} NMR (200 MHz, CDCl₃, 85% H₃PO₄): 98.37 (s) ppm. ¹³C{¹H} NMR (125 MHz, CDCl₃): 213.74, 213.67, 210.04 (C≡O), 150.19, 149.01, 148.92, 135.07, 134.71, 130.75, 130.56, 130.46, 129.02, 128.94, 113.09 (Ar–C), 34.96, 34.93 (CH₂) ppm.

3.7. Preparation of (μ -PDT)Fe₂(CO)₅[Ph₂PP(O)Ph₂] (**9**) and (μ -PDT)Fe₂(CO)₅(Ph₂PNHPy-4) (**10**)

The procedure was similar to that of **7** and **8** except **2** (0.386 g, 1 mmol) was used instead of **1**. 0.149 g (21%) of **9** and 0.242 g (38%) of **10** were obtained as red solids. **9**: Anal. Calc. for C₃₂H₂₆Fe₂O₆P₂S₂: C, 51.64; H, 3.52. Found: C, 51.89; H, 3.41%. IR (KBr disk): ν_{C≡O} 2041vs, 1985vs, 1948vs cm⁻¹. ¹H NMR (500 MHz, CDCl₃): 7.87–7.73 (m, 20H, Ar–H), 1.68–1.63 (m, 4H, 2SCH₂), 1.28–1.25 (m, 2H, SCH₂CH₂CH₂) ppm. ³¹P{¹H} NMR (200 MHz, CDCl₃, 85% H₃PO₄): 56.39 (d, J_{P–P} = 79.5 Hz), 34.61 (d, J_{P–P} = 79.5 Hz) ppm. ¹³C{¹H} NMR (125 MHz, CDCl₃): 211.61, 211.57, 209.05 (C≡O), 135.08, 134.99, 132.56, 132.48, 131.08, 128.49, 128.41 (Ar–C), 30.09 (s, SCH₂), 21.00 (s, SCH₂CH₂CH₂S) ppm.

3.8. Preparation of (μ -EDT)Fe₂(CO)₄(Ph₂PCH₂CH₂PPh₂) (**11**)

A mixture of **1** (0.186 g, 0.5 mmol), dppe (0.199 g, 0.5 mmol) and xylene (20 mL) was refluxed for 4 h to give a brown–red solution. The solvent was reduced *in vacuo* and the residue was subjected to TLC separation using CH₂Cl₂/petroleum ether (*v/v* = 1:1) as eluent. Collecting the main red band afforded 0.112 g (31%) of **11** as a red solid. Anal. Calc. for C₃₂H₂₈Fe₂O₄P₂S₂: C, 53.81; H, 3.95. Found: C, 53.52; H, 3.89%. IR (KBr disk): ν_{C≡O} 2017vs, 1955vs, 1929vs, 1896vs cm⁻¹. ¹H NMR (500 MHz, CDCl₃): 7.91–7.46 (m, 20H, Ar–H), 2.84–2.63 (m, 4H, PCH₂CH₂P), 1.75–1.74 (m, 2H, SCH₂), 1.22–1.20 (m, 2H, SCH₂) ppm. ³¹P{¹H} NMR (200 MHz, CDCl₃, 85% H₃PO₄): 91.58 (s) ppm.

3.9. Preparation of (μ -PDT)Fe₂(CO)₄[(η^5 -Ph₂PC₅H₄)₂Fe] (**12**)

The procedure was similar to that of **11** except **2** (0.192 g, 0.5 mmol) and dppf (0.278 g, 0.5 mmol) were used instead of **1** and dppe. 0.124 g (28%) of **12** was obtained as a red solid. Anal.

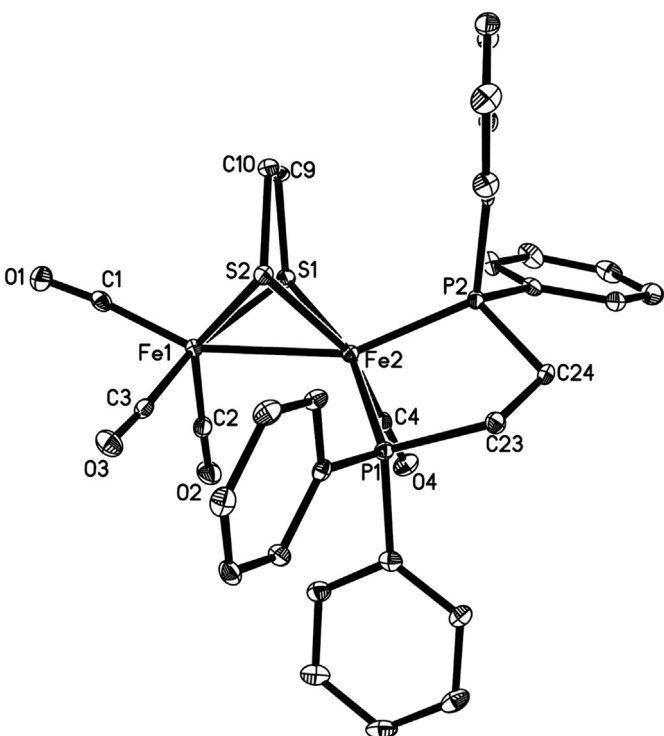


Fig. 7. ORTEP view of **11** with 30% probability level ellipsoids.

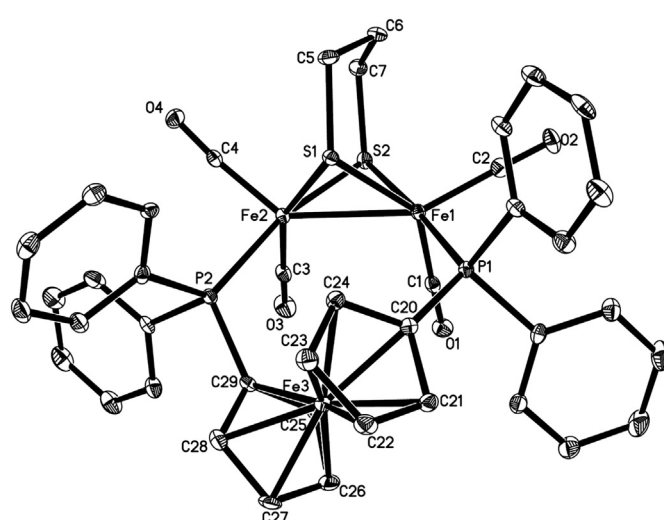


Fig. 8. ORTEP view of **12** with 30% probability level ellipsoids.

Table 4Crystal data and structure refinements details for **3–6**.

Complex	3	4	5	6
Empirical formula	C ₂₅ H ₁₉ Fe ₂ O ₅ PS ₂	C ₃₂ H ₂₆ Fe ₂ O ₅ P ₂ S ₂ ·CH ₂ Cl ₂	C ₁₂ H ₁₃ Fe ₂ NO ₅ S ₂	C ₁₆ H ₂₂ Fe ₂ N ₂ O ₄ S ₂
Formula weight	606.19	813.21	427.05	482.18
Temperature (K)	113(2)	113(2)	113(2)	113(2)
Wavelength (Å)	0.71073	0.71073	0.71073	0.71073
Crystal system	Monoclinic	Triclinic	Monoclinic	Monoclinic
Space group	P2(1)/c	P-1	C2/m	P2(1)/n
<i>a</i> (Å)	9.1711(18)	11.735(3)	14.441(17)	8.5993(18)
<i>b</i> (Å)	17.143(3)	11.766(3)	10.533(11)	16.447(4)
<i>c</i> (Å)	16.545(3)	12.540(4)	12.376(15)	15.120(3)
α (°)	90	86.880(11)	90	90
β (°)	103.555(4)	82.079(9)	113.323(14)	92.307(3)
γ (°)	90	80.772(10)	90	90
<i>V</i> (Å ³)	2528.7(8)	1691.8(8)	1729(3)	2136.6(8)
<i>Z</i>	4	2	4	4
<i>D</i> _{calc} (g cm ⁻³)	1.592	1.596	1.641	1.499
μ (mm ⁻¹)	1.410	1.274	1.937	1.575
<i>F</i> (000)	1232	828	864	992
Crystal size (mm ³)	0.24 × 0.20 × 0.10	0.26 × 0.20 × 0.10	0.20 × 0.18 × 0.12	0.20 × 0.18 × 0.10
θ _{min} , θ _{max} (°)	1.74, 27.87	1.64, 25.02	1.79, 29.00	1.83, 27.88
Reflections collected/unique	25,524/5988	14,262/5920	9097/2417	21,521/5087
<i>R</i> _{int}	0.0348	0.0741	0.0598	0.0365
<i>hkl</i> range	-11 ≤ <i>h</i> ≤ 12 -21 ≤ <i>k</i> ≤ 22 -21 ≤ <i>l</i> ≤ 21	-13 ≤ <i>h</i> ≤ 13 -13 ≤ <i>k</i> ≤ 13 -14 ≤ <i>l</i> ≤ 14	-19 ≤ <i>h</i> ≤ 19 -14 ≤ <i>k</i> ≤ 14 -16 ≤ <i>l</i> ≤ 16	-11 ≤ <i>h</i> ≤ 10 -21 ≤ <i>k</i> ≤ 21 -19 ≤ <i>l</i> ≤ 19
Completeness to θ _{max} (%)	99.4	99.5	99.8	99.6
Data/restraints/parameters	5988/0/316	5920/0/415	2417/12/114	5087/126/291
GOF on <i>F</i> ²	0.999	0.886	0.978	1.125
<i>R</i> 1/w <i>R</i> 2 (<i>I</i> > 2σ(<i>I</i>))	0.0271/0.0650	0.0353/0.0617	0.0315/0.0501	0.0323/0.0972
<i>R</i> 1/w <i>R</i> 2 (all data)	0.0335/0.0672	0.0479/0.0636	0.0491/0.0525	0.0387/0.0994
Δρ _{max/min} (e Å ⁻³)	0.472/-0.232	0.525/-0.510	0.483/-0.573	1.549/-0.468

Table 5Crystal data and structure refinements details for **7, 9, 11**, and **12**.

Complex	7	9	11	12
Empirical formula	C ₃₁ H ₂₄ Fe ₂ O ₆ P ₂ S ₂ ·CH ₂ Cl ₂	C ₃₂ H ₂₆ Fe ₂ O ₆ P ₂ S ₂ ·0.5CH ₂ Cl ₂	C ₃₂ H ₂₈ Fe ₂ O ₄ P ₂ S ₂ ·0.5CH ₂ Cl ₂	C ₄₁ H ₃₄ Fe ₃ O ₄ P ₂ S ₂ ·0.5CH ₂ Cl ₂
Formula weight	815.19	786.75	756.77	926.76
Temperature (K)	113(2)	113(2)	113(2)	113(2)
Wavelength (Å)	0.71073	0.71073	0.71073	0.71073
Crystal system	Monoclinic	Monoclinic	Monoclinic	Triclinic
Space group	Cc	C2/c	P2(1)/n	P-1
<i>a</i> (Å)	10.959(3)	35.538(7)	9.4212(19)	9.715(4)
<i>b</i> (Å)	20.626(6)	9.1927(15)	28.351(6)	13.143(5)
<i>c</i> (Å)	15.269(5)	21.873(4)	24.118(5)	16.645(6)
α (°)	90	90	90	99.663(6)
β (°)	93.600(6)	108.137(3)	96.582(4)	94.320(5)
γ (°)	90	90	90	111.344(4)
<i>V</i> (Å ³)	3444.7(17)	6791(2)	6400(2)	1929.9(12)
<i>Z</i>	4	8	8	2
<i>D</i> _{calc} (g cm ⁻³)	1.572	1.539	1.571	1.595
μ (mm ⁻¹)	1.254	1.193	1.258	1.416
<i>F</i> (000)	1656	3208	3096	946
Crystal size (mm ³)	0.20 × 0.18 × 0.16	0.20 × 0.18 × 0.12	0.30 × 0.10 × 0.10	0.20 × 0.18 × 0.14
θ _{min} , θ _{max} (°)	1.97, 25.02	1.21, 27.90	1.11, 25.02	1.70, 27.87
Reflections collected/unique	14,556/5686	30,520/8107	53,693/11,302	20,056/9032
<i>R</i> _{int}	0.0351	0.0534	0.0747	0.0401
<i>hkl</i> range	-13 ≤ <i>h</i> ≤ 13 -24 ≤ <i>k</i> ≤ 24 -18 ≤ <i>l</i> ≤ 17	-46 ≤ <i>h</i> ≤ 42 -12 ≤ <i>k</i> ≤ 10 -28 ≤ <i>l</i> ≤ 28	-11 ≤ <i>h</i> ≤ 11 -33 ≤ <i>k</i> ≤ 33 -28 ≤ <i>l</i> ≤ 28	-12 ≤ <i>h</i> ≤ 12 -17 ≤ <i>k</i> ≤ 17 -16 ≤ <i>l</i> ≤ 21
Completeness to θ _{max} (%)	100.0	99.7	99.9	98.2
Data/restraints/parameters	5686/2/415	8107/76/451	11,302/0/784	9032/0/487
GOF on <i>F</i> ²	1.043	1.033	1.156	1.023
<i>R</i> 1/w <i>R</i> 2 (<i>I</i> > 2σ(<i>I</i>))	0.0248/0.0423	0.0430/0.0832	0.0569/0.1008	0.0370/0.0988
<i>R</i> 1/w <i>R</i> 2 (all data)	0.0272/0.0426	0.0581/0.0930	0.0711/0.1059	0.0477/0.1015
Δρ _{max/min} (e Å ⁻³)	0.337/-0.278	0.765/-0.477	0.524/-0.615	0.575/-0.687

Calc. for C₄₁H₃₄Fe₃O₄P₂S₂: C, 55.69; H, 3.88. Found: C, 55.38; H, 4.16%. IR (KBr disk): ν_{C≡O} 1984vs, 1942vs, 1909vs, 1890vs cm⁻¹. ¹H NMR (500 MHz, CDCl₃): 8.03–7.26 (m, 20H, Ar–H), 4.93, 4.46, 4.45, 4.01 (4s, 8H, Cp–H), 2.60, 2.28, 2.13 (3s, 6H, 3CH₂) ppm. ³¹P {¹H} NMR (200 MHz, CDCl₃, 85% H₃PO₄): 50.85 (s) ppm. ¹³C{¹H} NMR

(125 MHz, CDCl₃): 216.16, 215.98, 215.47, 215.35 (C≡O), 141.06, 140.73, 138.07, 137.76, 135.04, 134.97, 131.13, 131.06, 129.71, 129.00, 127.83, 127.76, 127.55, 127.48 (Ar–C), 79.83, 79.56, 72.53, 72.50, 72.44, 72.41, 71.02, 70.99 (Cp–C), 31.14, 25.71, 22.86 (CH₂) ppm.

3.10. X-ray structure determinations of 3–7, 9, 11 and 12

Single crystals of **3–7, 9, 11** and **12** suitable for X-ray diffraction analysis were grown by slow evaporation of its $\text{CH}_2\text{Cl}_2/\text{hexane}$ solution at 4 °C. A single crystal of **3–7, 9, 11** or **12** was mounted on a Rigaku MM-007 CCD diffractometer. Data were collected by using a graphite monochromator with Mo-K α radiation ($\lambda = 0.71073 \text{ \AA}$) in the $\omega-\phi$ scanning mode. Absorption correction was performed by CRYSTALCLEAR program [42]. Both structures were solved by direct methods using the SHELXS-97 program [43] and refined by full-matrix least-squares techniques (SHELXL-97) [44] on F^2 . Hydrogen atoms were located using the geometric method. Details of crystal data, data collections, and structure refinements are summarized in Tables 4 and 5.

4. Conclusions

We have found that the new diiron dithiolate complexes **3–12** can be synthesized by carbonyl substitution reactions of parent complex **1** or **2** with monophosphines, diphosphines or isocyanide in the presence or absence of the decarbonylating agent $\text{Me}_3\text{NO} \cdot 2\text{H}_2\text{O}$ or at reflux in xylene. It is interesting to find out that unexpected products **7–10** were obtained by reactions of **1** or **2** with pyridyl-functionalized diphosphine 4-PyN(PPh_2)₂ in the presence of $\text{Me}_3\text{NO} \cdot 2\text{H}_2\text{O}$. The asymmetric diphosphine substituted complex **11** and the symmetric diphosphine substituted complex **12** were obtained by reactions of **1** or **2** with dppe or dppf at reflux in xylene. All complexes are structurally characterized by various spectroscopic methods and some of them by X-ray crystallography.

Acknowledgments

This work was supported by the National Training Programs of Innovation and Entrepreneurship for Undergraduates (201311058010), the Zhejiang Province Science and Technology Innovation Program (2013R422014), and Ningbo Science and Technology Innovation Team (2011B82002).

Appendix A. Supplementary material

CCDC 858685 (3), 858686 (4), 858684 (5), 858683 (6), 844821 (7), 834046 (9), 866144 (11) and 949417 (12) contain the supplementary crystallographic data for this paper. These data can be obtained free of charge from The Cambridge Crystallographic Data Centre via www.ccdc.cam.ac.uk/data_request/cif.

References

- [1] (a) D.J. Evans, C.J. Pickett, *Chem. Soc. Rev.* 32 (2003) 268–275;
 (b) C. Tard, C.J. Pickett, *Chem. Rev.* 109 (2009) 2245–2274.
- [2] F. Gloaguen, T.B. Rauchfuss, *Chem. Soc. Rev.* 38 (2009) 100–108.
- [3] J.-F. Capon, F. Gloaguen, F.Y. Pétillon, P. Schollhammer, J. Talarmin, *Eur. J. Inorg. Chem.* (2008) 4671–4681.
- [4] S.P.J. Albracht, *Biochim. Biophys. Acta Bioenerg.* 1188 (1994) 167–204.
- [5] E. Garcin, X. Verneude, E.C. Hatchikian, A. Volbeda, M. Frey, J.C. Fontecilla-Camps, *Structure* 7 (1999) 557–566.
- [6] Y. Nicolet, B.J. Lemon, J.C. Fontecilla-Camps, J.W. Peters, *Trends Biochem. Sci.* 25 (2000) 138–143.
- [7] A. Volbeda, J.C. Fontecilla-Camps, *Dalton Trans.* (2003) 4030–4038.
- [8] S. Shima, R.K. Thauer, *Chem. Rec.* 7 (2007) 37–46.
- [9] M.W.W. Adams, *Biochim. Biophys. Acta Bioenerg.* 1020 (1990) 115–145.
- [10] L.-C. Song, *Acc. Chem. Res.* 38 (2005) 21–28.
- [11] M. Frey, *ChemBioChem* 3 (2002) 153–160.
- [12] W. Lubitz, W. Tumas, *Chem. Rev.* 107 (2007) 3900–3903.
- [13] J.W. Peters, W.N. Lanzilotta, B.J. Lemon, L.C. Seefeldt, *Science* 282 (1998) 1853–1858.
- [14] Y. Nicolet, C. Piras, P. Legrand, E.C. Hatchikian, J.C. Fontecilla-Camps, *Structure* 7 (1999) 13–23.
- [15] (a) E.J. Lyon, I.P. Georgakaki, J.H. Reibenspies, M.Y. Darenbourg, *Angew. Chem. Int. Ed.* 38 (1999) 3178–3180;
 (b) Z. Xiao, Z. Wei, L. Long, Y. Wang, D.J. Evans, X. Liu, *Dalton Trans.* 40 (2011) 4291–4299;
 (c) P.-H. Zhao, Y.-Q. Liu, G.-Z. Zhao, *Polyhedron* 53 (2013) 144–149;
 (d) X.-F. Liu, B.-S. Yin, *J. Coord. Chem.* 63 (2010) 4061–4067;
 (e) S. Ghosh, G. Hogarth, N. Hollingsworth, K.B. Holt, I. Richards, M.G. Richmond, B.E. Sanchez, D. Unwin, *Dalton Trans.* 42 (2013) 6775–6792.
- [16] (a) J.D. Lawrence, H. Li, T.B. Rauchfuss, M. Bénard, M.M. Rohmer, *Angew. Chem. Int. Ed.* 40 (2001) 1768–1771;
 (b) X.-F. Liu, X.-W. Xiao, L.-J. Shen, *J. Coord. Chem.* 64 (2011) 1023–1031;
 (c) X.-F. Liu, X.-W. Xiao, L.-J. Shen, *Transition Met. Chem.* 36 (2011) 465–469.
- [17] L.-C. Song, Z.-Y. Yang, H.-Z. Bian, Q.-M. Hu, *Organometallics* 23 (2004) 3082–3084.
- [18] (a) C.A. Boyke, T.B. Rauchfuss, S.R. Wilson, M.M. Rohmer, M. Bénard, *J. Am. Chem. Soc.* 126 (2004) 15151–15160;
 (b) X.-F. Liu, Z.-Q. Jiang, Z.-J. Jia, *Polyhedron* 33 (2012) 166–170.
- [19] A. Jablonskyte, J.A. Wright, C.J. Pickett, *Eur. J. Inorg. Chem.* (2011) 1033–1037.
- [20] K. Charreteur, J.-F. Capon, F. Gloaguen, F.Y. Pétillon, P. Schollhammer, J. Talarmin, *Eur. J. Inorg. Chem.* (2011) 1038–1042.
- [21] S. Lounissi, J.F. Capon, F. Gloaguen, F. Matoussi, F.Y. Pétillon, P. Schollhammer, J. Talarmin, *Chem. Commun.* 47 (2011) 878–880.
- [22] X.-F. Liu, B.-S. Yin, Z. Anorg. Allg. Chem. 637 (2011) 377–379.
- [23] P.C. Ellgen, J.N. Gerlach, *Inorg. Chem.* 12 (1973) 2526–2532.
- [24] G. Hogarth, S.E. Kabir, I. Richards, *Organometallics* 29 (2010) 6559–6568.
- [25] A. Winter, L. Zsolnai, G. Huttner, *Z. Naturforsch. 37b* (1982) 1430–1436.
- [26] L.-C. Song, Q.-S. Li, Z.-Y. Yang, Y.-J. Hua, H.-Z. Bian, Q.-M. Hu, *Eur. J. Inorg. Chem.* (2010) 1119–1128.
- [27] B.-S. Yin, T.-B. Li, M.-S. Yang, *J. Coord. Chem.* 64 (2011) 2066–2074.
- [28] X.-F. Liu, *Inorg. Chim. Acta* 378 (2011) 338–341.
- [29] W. Gao, J. Ekström, J. Liu, C. Chen, L. Eriksson, L. Weng, B. Åkermark, L. Sun, *Inorg. Chem.* 46 (2007) 1981–1991.
- [30] M.C. Ortega-Alfaro, N. Hernández, I. Cerna, J.G. López-Cortés, E. Gómez, R.A. Toscano, C. Alvarez-Toledo, *J. Organomet. Chem.* 689 (2004) 885–893.
- [31] J.L. Nehring, D.M. Heinekey, *Inorg. Chem.* 42 (2003) 4288–4292.
- [32] L.-C. Song, Z.-Y. Yang, Y.-J. Hua, H.-T. Wang, Y. Liu, Q.-M. Hu, *Organometallics* 26 (2007) 2106–2110.
- [33] X.-F. Liu, X.-W. Xiao, *J. Organomet. Chem.* 696 (2011) 2767–2771.
- [34] F. Huo, J. Hou, G. Chen, D. Guo, X. Peng, *Eur. J. Inorg. Chem.* (2010) 3942–3951.
- [35] S. Ott, M. Kritikos, B. Åkermark, L. Sun, R. Lomoth, *Angew. Chem. Int. Ed.* 43 (2004) 1006–1009.
- [36] S. Ezzaher, J.-F. Capon, F. Gloaguen, F.Y. Pétillon, P. Schollhammer, J. Talarmin, *Inorg. Chem.* 46 (2007) 3426–3428.
- [37] S. Ezzaher, J.-F. Capon, F. Gloaguen, F.Y. Pétillon, P. Schollhammer, J. Talarmin, *Inorg. Chem.* 46 (2007) 9863–9872.
- [38] S. Ezzaher, J.-F. Capon, F. Gloaguen, N. Kervarec, F.Y. Pétillon, R. Pichon, P. Schollhammer, J. Talarmin, C. R. Chimie 11 (2008) 906–914.
- [39] C.A. Mebi, B.C. Noll, R. Gao, D. Karr, Z. Anorg. Allg. Chem. 636 (2010) 2550–2554.
- [40] N. Biricik, F. Durap, C. Kayan, B. Gümgüm, N. Gürbüz, I. Özdemir, W.H. Ang, Z. Fei, R. Scopelliti, *J. Organomet. Chem.* 693 (2008) 2693–2699.
- [41] J.J. Bishop, A. Davison, M.L. Katcher, D.W. Lichtenberg, R.E. Merrill, J.C. Smart, *J. Organomet. Chem.* 27 (1971) 241–249.
- [42] CRYSTALCLEAR 1.3.6, Rigaku and Rigaku/MSC, The Woodlands, TX, 2005.
- [43] G.M. Sheldrick, SHELXS97, a Program for Crystal Structure Solution, University of Göttingen, Germany, 1997.
- [44] G.M. Sheldrick, SHELXL97, a Program for Crystal Structure Refinement, University of Göttingen, Germany, 1997.